Chapter 5
Sundry Specialized CELD Microstructures

5.1 Anodic Aluminum Oxide (AAO) Templated Nanowires

Due to their small sizes and potential for controllable features, nanowires/tubes represent an attractive option for increasing the surface area of ceria-based anodes. Templated approaches are currently the most flexible routes to fabricating nanowires/tubes, as only a suitable filling method needs be developed for a particular material composition, be it metallic, semiconducting, or ceramic, and so on. Anodic aluminum oxide (AAO) templates are utilized here for their uniformity and tunability. The AAO template fabrication process is first discussed, and then the CELD of ceria into its pores is investigated.

5.1.1 *AAO Template Formation Mechanism and Background*

Aluminum naturally forms a thin oxide layer at room temperature and ambient atmospheres. Given an extra driving force and a much different environment, this oxide layer can take on a regular porous structure. Specifically, anodically oxidizing aluminum metal in a liquid acidic electrolyte can produce an oxide layer with in-plane, hexagonally arranged and vertically aligned pores (see the schematic in Fig. 5.1 and SEM images in Fig. 5.2). The pores are straight and extend throughout the entire thickness of the oxide, with the exception of a small “barrier layer” lying at the bottom of the pores, at the metal|oxide interface. The geometric ratios of the structural features are primarily

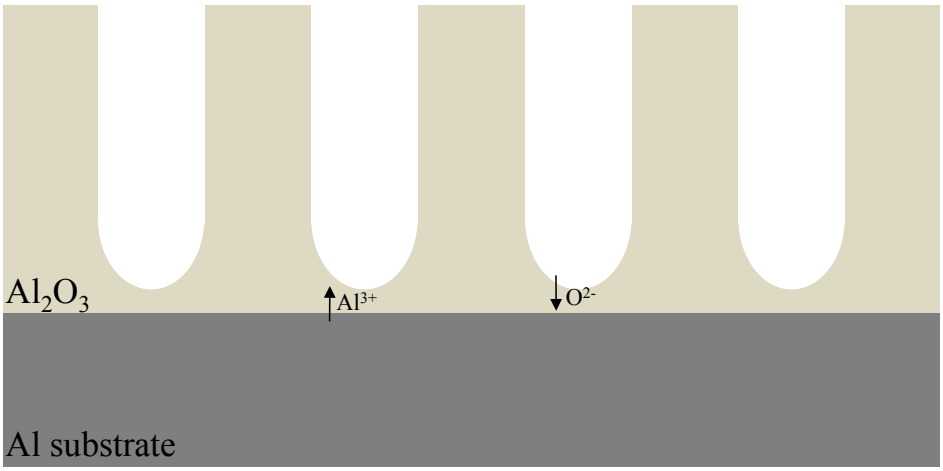

Fig. 5.1. A schematic showing a cross-sectional view of the hexagonally arrayed, vertically aligned porous oxide template produced by anodically oxidizing aluminum metal. Aluminum ions generally travel toward the liquid acidic electrolyte and oxygen ions from solution toward the positively biased aluminum metal. An oxide barrier layer exists at the bottom of each pore.

controlled by the applied voltage—the diameter, inter-pore spacing, and even barrier layer thickness all linearly depend on the voltage. In addition, different electrolyte solution compositions provide different feature size ranges and, hence, different operating voltage ranges. The three most common electrolyte solutions in ascending feature size order are sulfuric acid, oxalic acid, and phosphoric acid.

Since the initial investigations began in the 1940's [98-99], attempts have been made to explain the seemingly anomalous behavior of the formation of porous alumina. Recently, a comprehensive picture has been given that adequately explains the formation mechanism and describes the steady-state growth conditions, mainly by uniting the early theories [100-103]. The conclusions presented in the preceding references are summarized below. First, the two governing reactions are given—aluminum ion

generation at the metal|oxide interface, and oxygen ion deposition at the oxide|electrolyte solution interface.

$$Al \rightarrow Al^{3+} + 3e^{-} \quad (5.1)$$

$$H_2O \rightarrow O^{2-}(ox) + 2H^{+}(aq) \quad (5.2)$$

Electric species migration is no doubt happening—the oxide layer continues to thicken and the aluminum metal is consumed as long as a voltage is applied. Although the exact origin of the localized effects that ultimately lead to pore formation is not well-understood, it is now known that compressive stresses at the oxide|electrolyte solution interface induce significant steady-state lateral flow in the oxide, in directions perpendicular to the applied electric field. These stresses appear to come from competitive adsorption of oxygen ions, as in Eqn. 5.2, and anions from the electrolyte solution. The adsorption step highly regulates the current density, as well as impacts the lateral Newtonian flow of the oxide layer, accounting for the extreme dependence of the template geometry on electrolyte solution composition. This also explains why certain acids, such as boric acid, produce dense, planar oxide films under identical conditions as AAO template-producing acidic electrolyte solutions. The viscous flow induced by local stress concentration acts to push oxide material radially away from the pore bottoms, and then up the pore walls, and is ultimately restricted by volume expansion and charge conservation. The cascading effect of the applied voltage on the current density, adsorption rate, local stress formation, and lateral flow of the oxide explains its robust relationship to the geometric feature sizes of the resulting template.

Historically, it has been theorized that the pores were formed simply as a result of the applied voltage leading to local electric field-assisted dissolution of the oxide layer by

Joule (or, resistive) heating. Although this theory alone is unable to explain the invariance of the barrier layer thickness with time, it is a mechanistic factor, as it can lead to inhomogeneity in oxide formation rates for different regions of a single sample [103]. For bulk aluminum samples, Joule heating effects are unnoticeable. However, for thin film aluminum samples, which contain a buried gold or platinum under-electrode, rapid oxide dissolution arising from poor heat conduction of the supporting substrate can expose the gold/platinum to the liquid electrolyte. At operating voltages of 20 – 100 V, this translates into violent gaseous evolution catastrophically destroying the fragile thin film configuration.

5.1.2 *AAO Fabrication Experimental Details*

A two-electrode setup is used, with an HP 6002A DC Power Supply as the voltage source, aluminum metal (exposed surface area 0.5 – 2 cm^2) as the anode, and a carbon rod cathode, all immersed in an oxalic acid (0.3 – 0.6 M) liquid electrolyte. All anodizations are conducted at 40 V and room temperature. Under these conditions, the as-fabricated pore diameters are 15-25 nm, the inter-pore distance is ~90 nm, and the barrier layer thickness is ~25 nm. To open up the pore diameters, an etching solution of 10 wt % phosphoric acid is used for 10-30 minutes at 30 °C, giving final pore diameters of 40 – 80 nm.

Immediately upon applying a potential, the aluminum is anodically polarized, and aluminum oxide spontaneously and continuously forms until the voltage is turned off. This naturally consumes some depth of the aluminum metal, and for bulk aluminum samples, AAO templates of almost arbitrary thickness can be achieved. The template

thickness naturally depends on the anodization time, with a formation rate of 3 – 4 nm sec^{-1}. Free-standing templates can be produced by anodizing for a couple of hours, which gives a template thickness in the tens of microns range. To separate the oxide from the metal, a saturated solution of $HgCl_2$ is used to selectively attack the remaining aluminum metal, while the AAO template is undisturbed.

The oxalic acid electrolyte solution does etch the alumina and the aluminum metal during anodization, so a protective quick-drying coating (nail polish) is applied to the meniscus area, as the dissolution activity is greatly enhanced there. In some circumstances without this protective coating, a 0.25 mm thick aluminum foil sample could be entirely etched through, after only a couple hours of anodizing.

Although not a strict requirement for the simple goal of surface area enhancement, an ordered arrangement of pores is desirable, as a more accurate determination of the specific increase in surface area can be calculated. To accomplish this, a two-step anodization process is employed. First, an initial AAO layer is produced at 40 V for 10 minutes. This layer is subsequently removed in a combination of chromic (1.5 wt %) and phosphoric (6 wt %) acid at 60 °C, typically for 1 – 2 hours, depending on the AAO layer thickness. This leaves indentations in the newly-exposed aluminum surface. A second anodization at 40 V is then conducted, which produces the desired ordered arrangement, utilizing the existing indentations as nucleation points. Finally, the pore diameters are etched as before.

Conveniently, there is little variation in the produced structure when forming an AAO template over small or large areas, and there is obvious symbiotic potential for utilizing this liquid, electrochemical technique with other similar methods for ultimately

depositing nanowires, such as the CELDs of Chapter 3. Ultimately, the goal is to grow ceria nanowires onto an existing two-dimensional porous metal network, as in the anti-dot films of Chapter 2. A gradual, graded experimental approach was taken to gather critical criteria for successful AAO template growth in simple systems, before more complex systems were attempted. For the former, 0.25 mm thick bulk aluminum foil is used; for the latter, a thin film of aluminum (0.5 – 2 μm) is either thermally evaporated or sputtered onto a non-porous thin film of gold/titanium, which itself is thermally evaporated onto a robust substrate such as quartz, silicon, or YSZ. The titanium layer is only 10 nm thick, and is used strictly for adhesion improvement of the gold thin film. Because significant difficulties were encountered with this intermediate system, limited attempts were made to fabricate thin AAO template layers on anti-dot films.

5.1.3 *AAO Template Results*

The twice-anodized AAO template process is illustrated in Figure 5.2 for a bulk aluminum foil sample. As can be seen in Fig. 5.2a, the initial pore formation in the first anodization is highly irregular. As the anodization continues, however, a more homogeneous arrangement emerges. The first anodization should be conducted long enough to reach this homogeneous state—10 minutes is sufficient for the conditions given above. Fig. 5.2b shows the result of this evolution, where the first oxide layer has been removed, and a hexagonal configuration of indentations can be seen on the surface of the exposed aluminum metal. The chromic/phosphoric acid mixture used to remove the first anodization layer does not appreciably attack the aluminum over the etching time scales used here. Fig. 5.2cd show the ordered template after the second anodization

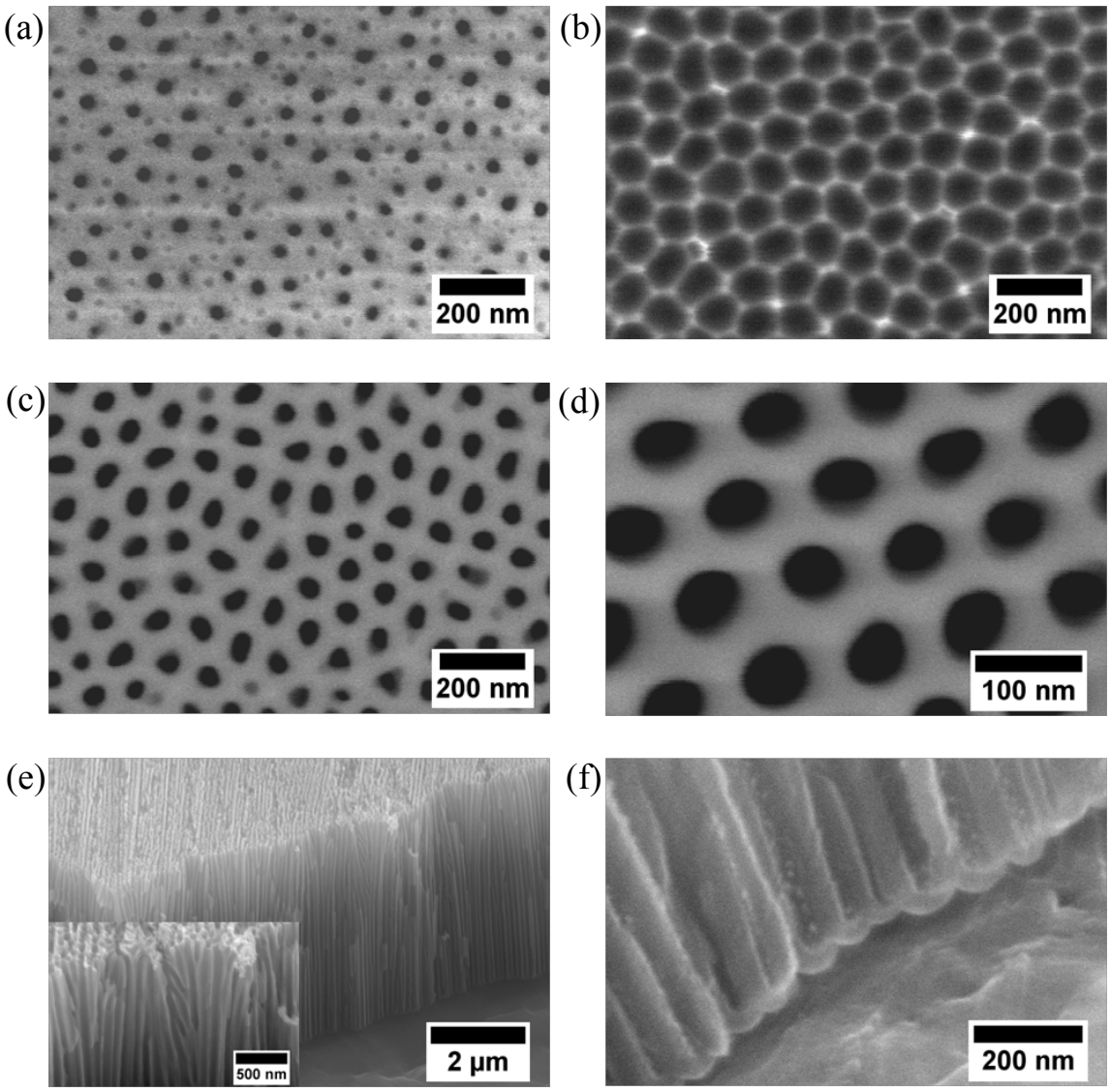

Fig. 5.2. SEM images showcasing the two-step anodization procedure (see text for experimental details): (a) a top-down view of the as-fabricated irregular pore growth after the first anodization; (b) after the first anodized oxide layer is removed, periodic depressions can be seen on the newly exposed aluminum metal surface; (c) and (d) top-down views of the second anodization layer after pore opening in phosphoric acid; (e) a cross-sectional view of the pores; and (f) the barrier layers at the bottoms of the pores of the second anodization oxide layer.

and pore etching steps, where the indentation effect from the first anodization can be clearly seen. A cross-sectional view of a thick template is seen in Fig. 5.2e, with an inset displaying some branched pores alongside perfectly aligned ones. Fig. 5.2f shows the unmistakable barrier layer at the bottom of each pore.

No inherent limitation to the thickness of the AAO template was encountered; nonetheless, relatively conservative thicknesses were investigated here, as maintaining contact between as-produced nanowires and the substrate is imagined to be more difficult the larger the aspect ratios are (the aspect ratio is the ratio of the length to the diameter). The other factor affecting the aspect ratio is the pore diameter—a corresponding comparison of different pore diameter etching times is shown in Figure 5.3. This etching

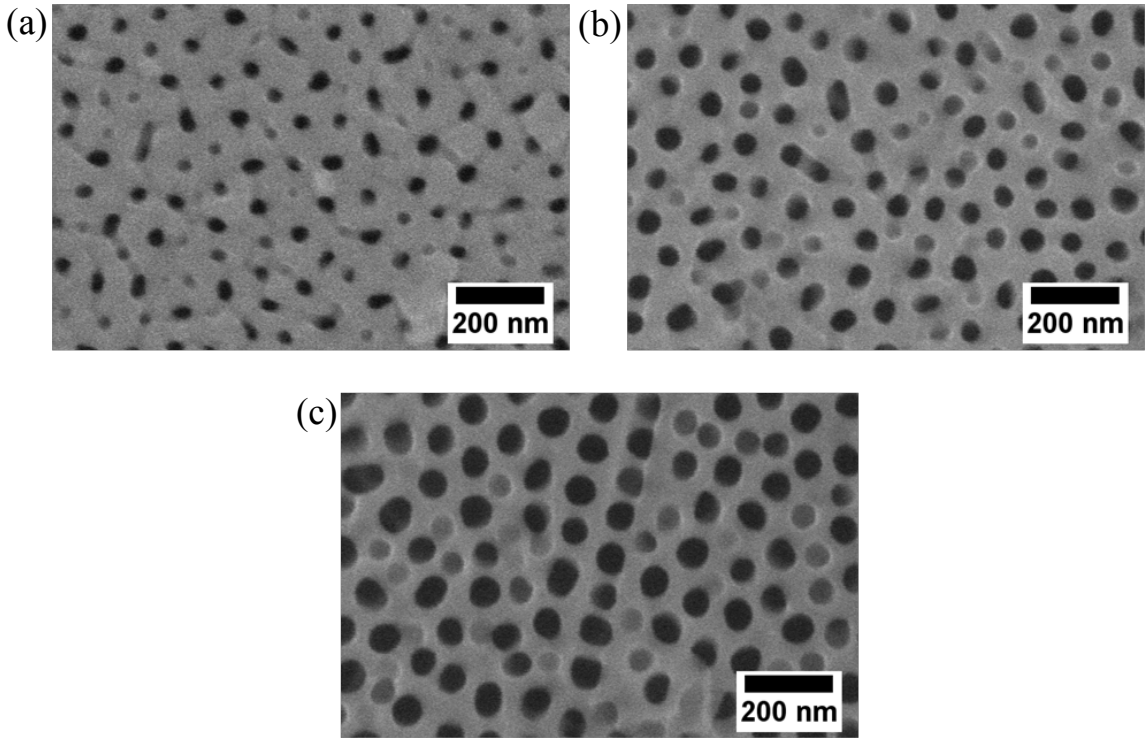

Fig. 5.3. SEM images of a twice-anodized template layer with different etching times in 10 wt % phosphoric acid: (a) 10 minutes, (b) 20 minutes, and (c) 30 minutes.

action also removes the barrier layer lying at the bottom of the pores. Without its removal, the barrier layer would cover all of the base electrogeneration sites, preventing the CELD of ceria nanowires.

Similar results to bulk aluminum are shown for sputtered aluminum thin film samples in Figure 5.4. The slight roughness pictured in Fig. 5.4b is a result of the sputtering process, which sometimes deposits large chunks of aluminum, instead of the expected flat and featureless film. The pores can be seen to run right down to the underlying gold surface. Either gold or platinum must be used as the buried electrode, because other non-precious metals would be too easily oxidized, as aluminum is.

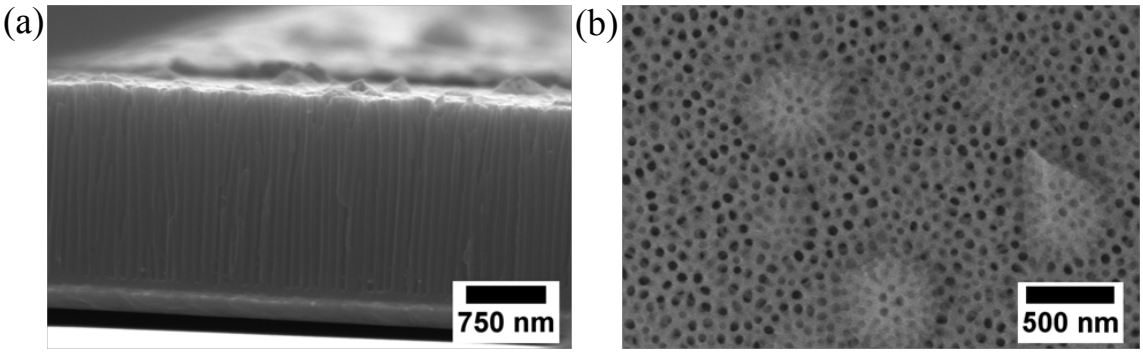

Fig. 5.4. SEM images of an AAO template grown from a sputtered aluminum thin film on a gold/titanium buried electrode on a silicon substrate. The pore opening was performed for 20 minutes.

Two prohibitive difficulties were encountered for the aluminum thin film samples. The first is inhomogeneous current densities arising from poor heat dissipation by the supporting substrate, as discussed in Section 5.1.1. Because of this issue, successful thin film AAO template fabrication was less than 1 in 10. Figure 5.5 compares three different quartz substrate thin film samples, with a corresponding current transient taken during each anodization. The first sample contains no buried gold electrode under

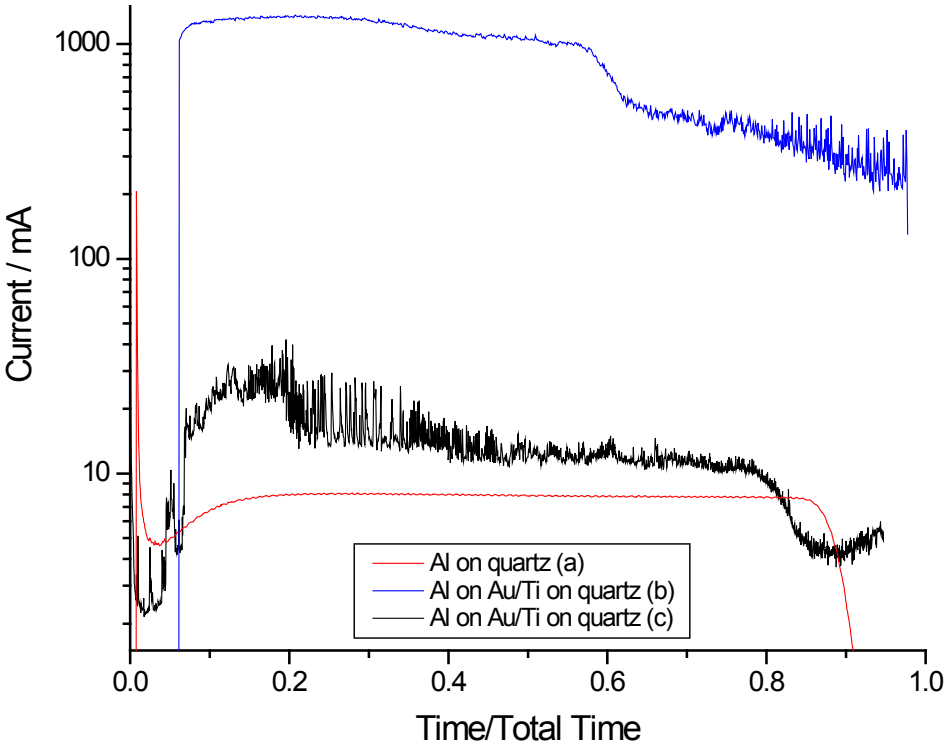

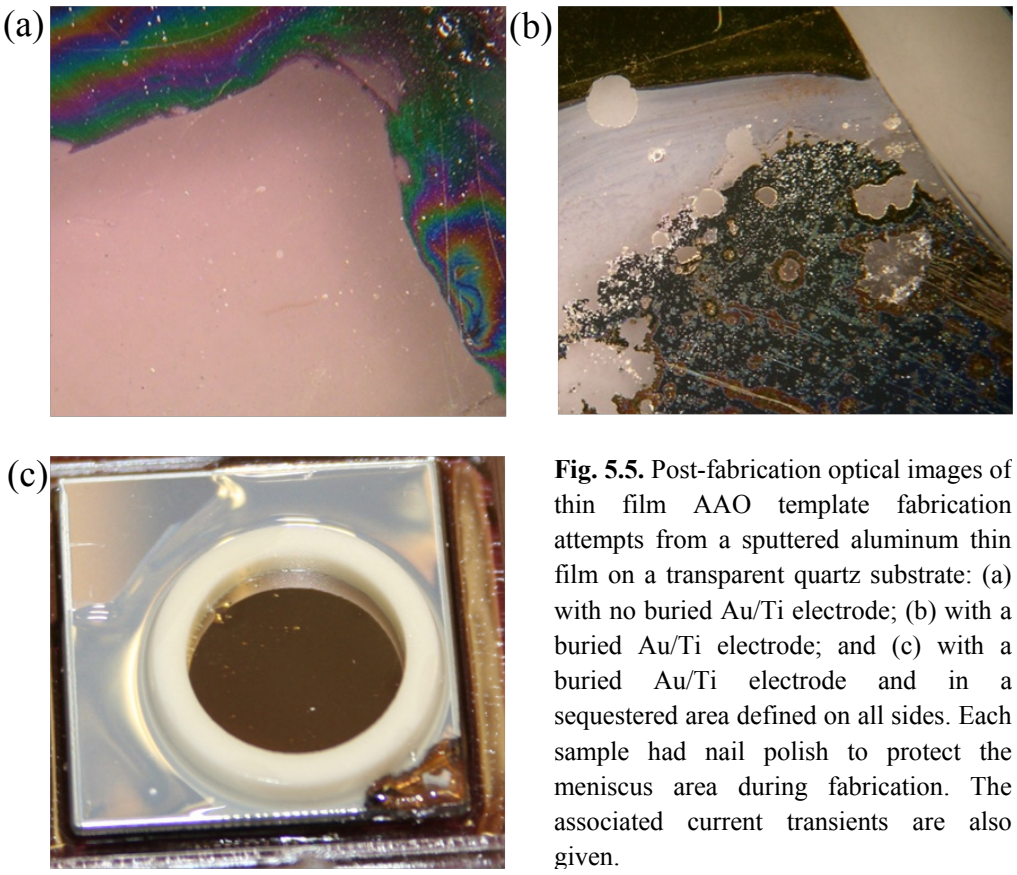

Fig. 5.5. Post-fabrication optical images of thin film AAO template fabrication attempts from a sputtered aluminum thin film on a transparent quartz substrate: (a) with no buried Au/Ti electrode; (b) with a buried Au/Ti electrode; and (c) with a buried Au/Ti electrode and in a sequestered area defined on all sides. Each sample had nail polish to protect the meniscus area during fabrication. The associated current transients are also given.

the sputtered aluminum thin film, but still experienced complete oxidation, resulting in the transparent window pictured in the top down view of Fig. 5.5a. Partial oxidation of the aluminum around the border of the sectioned area can be seen manifesting by colorful thin film interference patterns. This sample's current transient is a standard anodization response: after the initial charging current spike, a slight dip in the current is followed by a flat steady-state value, until there is no more aluminum to oxidize and the current drops to zero. In contrast, the sample pictured in Fig. 5.5b contains a buried gold electrode, where violent gaseous evolution can be seen to have ripped apart portions of the film, leaving the gold under-electrode completely exposed in some regions. The corresponding current transient shows orders of magnitude difference in the absolute current values, as well as undesirable spiking. The added current is coming from electrolytic oxidation reactions taking place at exposed gold surfaces. Finally, a successful buried gold electrode sample is shown in Fig. 5.5c, where the sectioned area for anodization is a bronze color, in stark contrast to the protected, un-oxidized aluminum surrounding it. This sample's current transient bears more resemblance to the first, although some variability still exists, largely due to the lower right-hand corner of the sample not being protected enough. Similar to the sample with no buried gold electrode, the current drops significantly when there is no more aluminum to oxidize.

A similar difficulty was reported in ref [103], utilizing a buried gold electrode thin film configuration. To alleviate the problem, the anodization was carried out at ~5 °C, and a pulsed voltage profile was employed, to allow time for any heat intensity to dissipate. An analogous approach could be taken here.

The second issue is related to the barrier layer, shown for a bulk aluminum foil sample in Fig. 5.6a and for a thin film sample in Fig. 5.6b. Note the thickness difference in the barrier layers—the thin film sample has a much thicker barrier layer. Even after etching, this barrier layer does not appear to be completely removed, which precludes subsequent ceria CELD into the pores. This could be related to the non-zero final current value recorded for the sample pictured in Fig. 5.5c. The stray current could be oxidizing some gold metal, producing what appears to be a thicker barrier layer. Nevertheless, this should not be an insolvent issue, as there are many reports of successful nanowire depositions in this configuration, as discussed below.

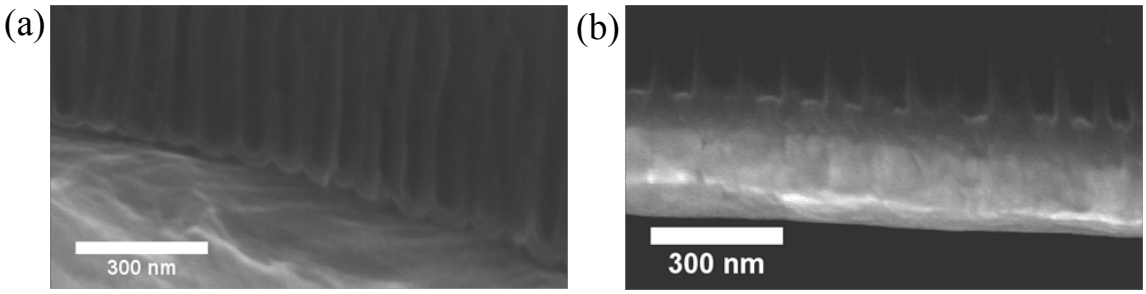

Fig. 5.6. SEM images comparing barrier layer thicknesses: (a) ~30 nm from a bulk aluminum foil sample; and (b) ~70 nm from a thin film sputtered aluminum sample.

5.1.4 *Ceria Nanowire Growth*

Aside from ceria [47, 49, 58-59, 81], a wide range of metals and semiconductors have been grown in the pores of AAO templates, from nickel to titania [104-110]. Despite numerous reports of successful electrochemical nanowire deposition into thin film AAO on a conducting substrate, the problems mentioned in the previous section have not been solved here, as of yet. To circumvent those two issues entirely and demonstrate a proof-of-concept, nickel metal was sputter-coated onto one side of a free-standing AAO template (Whatman Anodisc 47) with ~200 nm pore diameters. This template was then attached to a glass slide via conducting copper tape and sealed with nail polish, leaving ~1 cm^2 of an exposed surface. After allowing the electrolyte solution to naturally seep into the AAO pores for ~30 minutes, CELD was performed galvanostatically at 1.6 mA cm^{-2}, for 30 minutes. After the deposition was complete, the alumina was etched in stages in 3 M NaOH for 0.5 – 5 minutes. The resulting SEM images are shown in Figure 5.7.

The proportion of pores that are filled with CELD ceria is extremely high—it was difficult to find a pore that is not filled. After etching, the nanowires appear to fall onto each other, clumping up in sections. Although this result is not ideal for pure surface area enhancement, some cross-linking of nanowires could have a beneficial effect for assisting the lateral migration of active species, rather than requiring electrons and oxygen ions to always traverse the length of the nanowire during fuel cell operation.

The entire assembly was also subjected to thermal treatment, to observe the morphological stability of the nanowires. Figure 5.8 shows identically magnified images of the nanowires after annealing at 300 and 500 °C for 5 hours at 5 °C min^{-1}, revealing

that there is little to no evolution in the nanowires' structure at these temperatures. This is consistent with the high temperature results from Chapter 3, where much smaller features were shown to be stable up to ~800 °C.

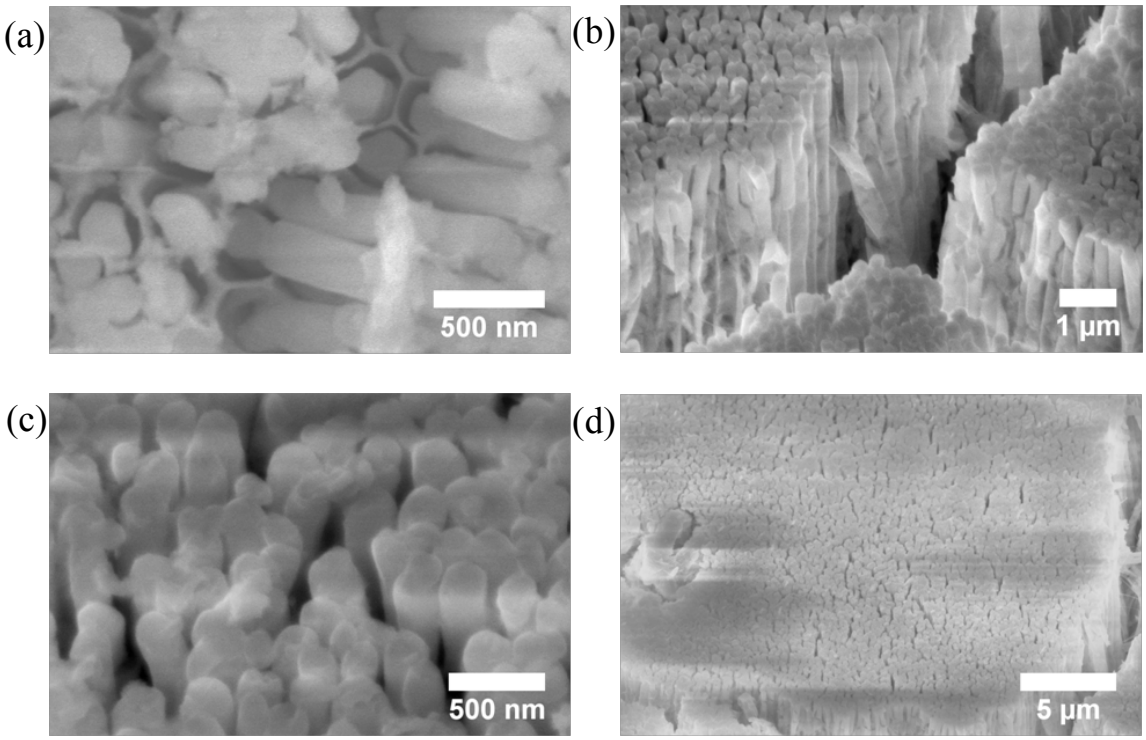

Fig. 5.7. SEM images of CELD nanowires grown in the pores of a free-standing AAO template after etching in 3 M NAOH: (a) for 30 seconds and showing a top-down view; and (b-d) for 5 minutes, showing angled views of various magnifications.

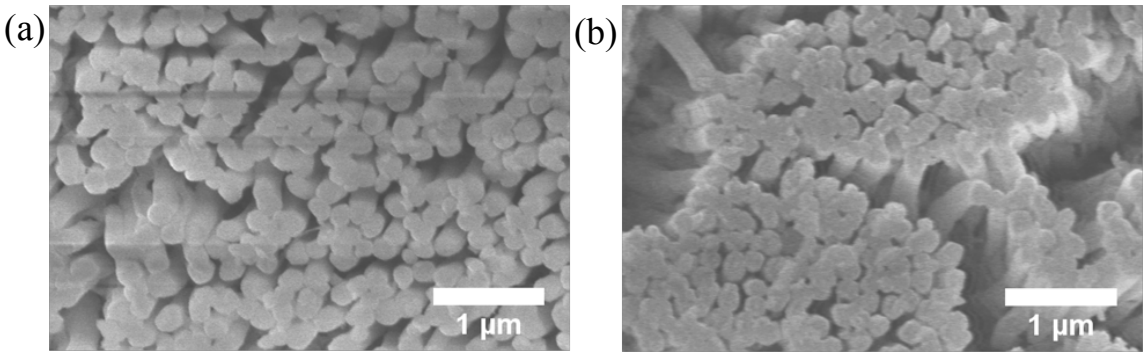

Fig. 5.8. SEM images of CELD nanowires grown in the pores of a free-standing AAO template after annealing for 5 hours in air at (a) 300 °C and (b) 500 °C.

5.2 Inverse Opals

5.2.1 *Inverse Opal Definition and Background*

Nanowires are an effective way to increase surface area, but they are limited to reasonable aspect ratios due to both the ability of the nanowires to stand relatively upright, and the challenges of depositing several microns of aluminum metal that would be required to make AAO templates thick enough to guide such growth. Indeed, the potential electrochemically active space is generally assumed to be on the order of 10 microns perpendicularly away from the electrolyte layer in SOFCs. A large portion of this volume would essentially remain unused in a nanowire-only design.

Another possibility is the inverse opal structure, schematically shown in Fig. 1.5cd. An opal structure is comprised of a three-dimensional close-packing of monodisperse spheres, akin to a micro-sized face-centered cubic structure. An inverse opal is the volume inverse of this close-packed monolith. Typically, one begins with an opal structure, deposits the desired material in the interstices of the opal, and then removes the original opal, leaving a well-defined inverse opal. Spheres with different diameters can be utilized to create a range of three-dimensional surface area enhancement, analogous to the two-dimensional variability shown for anti-dot metal films in Chapter 2 (c.f. Fig. 2.2). Polystyrene (PS) spheres are used here, although both poly(methyl methacrylate) and silica spheres are commonly used.

Any number of fluid based methods can be utilized to fill the interstices of the sacrificial opal structure, from gaseous CVD processes to liquid precursor infiltration techniques [111]. Perhaps the most popular infiltration route for metallic inverse opals is electrodeposition [112-117]; for ceria, most reports utilize techniques based upon

common ceria sol-gel precursors such as alkoxides and chlorides [118-121]. To the author's knowledge, no reports exist at the time of this writing for ceria inverse opal preparation by CELD.

5.2.2 *Inverse Opal Fabrication Details*

In keeping with CELD and SOFC configurational requirements, the familiar porous metal networks on YSZ are used as substrates. To establish a PS opal on the substrate, ~45 μL of a 10 wt % PS suspension is drop-cast onto a metal network/YSZ substrate and allowed to naturally dry for ~1 hour. Although this produces a randomly arranged opal, ordering is not crucial for surface area enhancement, just as with the CELD ceria nanowires of Section 5.1. After the water from the PS suspension is completely evaporated away, the resulting PS opal adheres nicely to the substrate. The entire assembly is then immersed into an undoped liquid electrolyte in the same CELD system used for the depositions of Chapter 3. Before the depositing potential is applied, ~30 minutes is given to allow the electrolyte solution to adequately infiltrate all interstices of the opal, and afterwards ceria is electrochemically deposited as before for 10-30 minutes. The PS spheres are initially removed by extensive water washing post-deposition, and can be completely removed by immersion in a toluene solution for 30 minutes, or thermal treatment at ~400 °C.

5.2.3 *Inverse Opal Results*

Figure 5.9 shows ceria inverse opal structures grown by CELD on platinum strip/YSZ (Fig. 5.9a-c) and nickel anti-dot/YSZ substrates (Fig. 5.9d) with HSA deposition conditions, i.e., 0.8 mA cm^{-2} with the undoped electrolyte solution. An advantage of

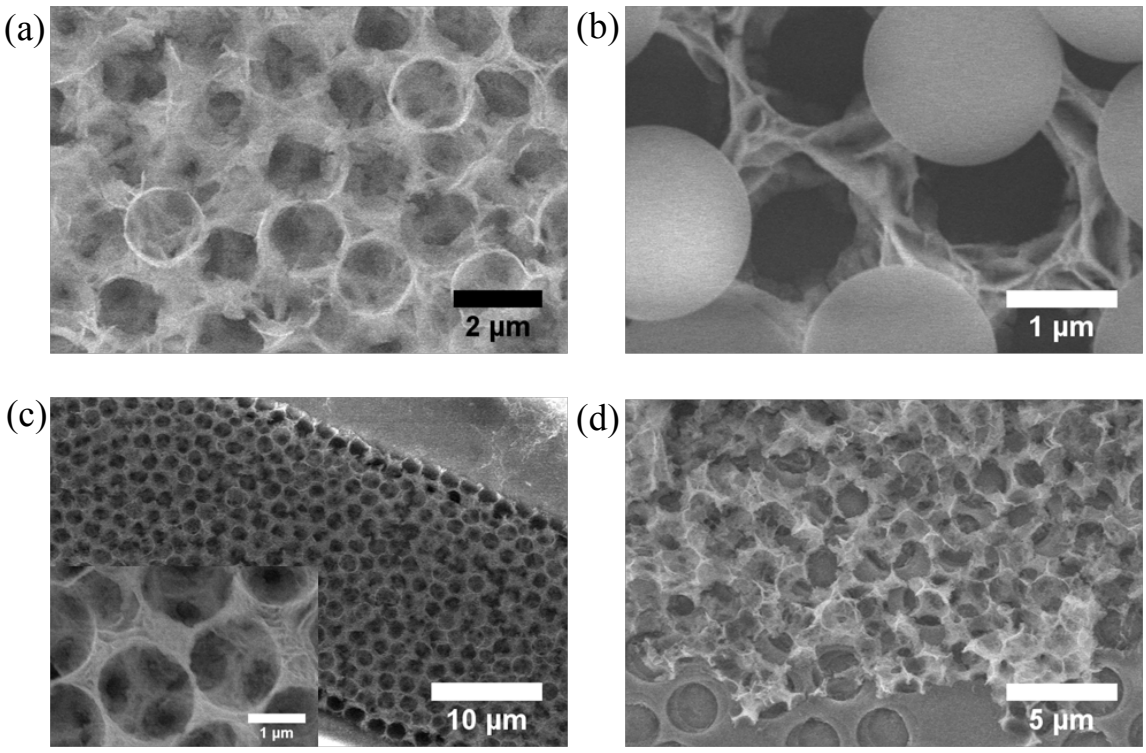

Fig. 5.9. SEM images of CELD inverse opal structures grown at 0.8 mA cm^{-2} with the undoped electrolyte on (a-c) a 20-20 µm YSZ/Pt strip sample for 10 minutes and (d) on a YSZ/Ni anti-dot substrate for 30 minutes. Immersion in a toluene solution for 30 minutes removed all PS spheres.

depositing at the standard HSA potentials is nano-sized surface area enhancement in addition to the micron-sized templated pores. The familiar nano-sheet/needle features can be seen embedded in the inverse opal walls in Fig. 5.9b and the inset of 5.9c. A 10 minute deposition produced 1-2 inverse opal layers for the platinum strip sample, and a 30 minute deposition produced 3-4 layers for the nickel anti-dot sample.

Two adhesion-related difficulties require further investigation. One, the PS opal consistently sticks to the substrate if unperturbed; however, when immersing the substrate/opal assembly into the CELD electrolyte solution, some of the opal becomes detached. The result is non-templated deposition, as in Fig. 5.10a. Two, the adhesion of

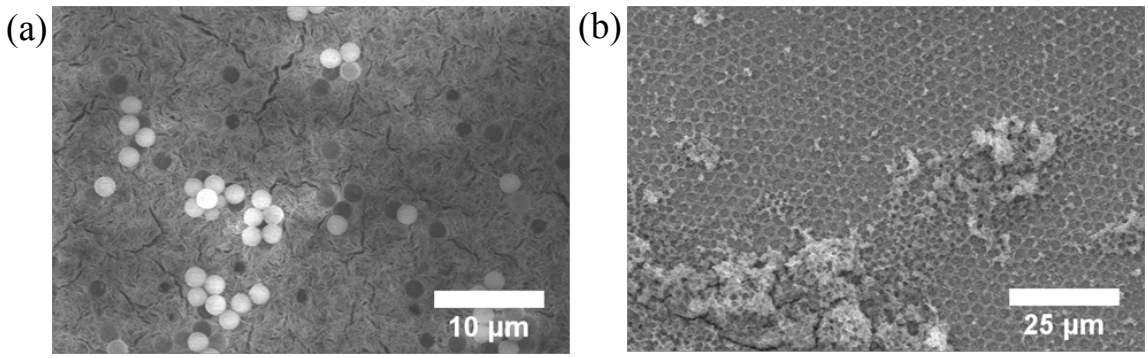

Fig. 5.10. SEM images of difficulties encountered with the CELD inverse opal structures from Fig. 5.9: (a) the PS opal structure can be accidentally removed when dipped into the liquid CELD electrolyte, and no inverse opal results; and (b) few contact points between the CELD inverse opal and the substrate can lead to spallation.

the ceria inverse opal to the substrate can be weak due to limited points of contact resulting from the template action of the PS spheres. Fig. 5.10b shows such a situation, where some of the inverse opal structure on a nickel anti-dot substrate spalled during the relatively gentle post-deposition water washing step. As is the case with the nanowire challenges posed in Section 5.1, these problems are solvable.

5.3 Oxidation Protection Coatings

Because of its ability to conformally coat irregularly shaped metallic substrates, CELD of ceria has been previously investigated as a corrosion inhibitor [46, 53-56]. Specifically relevant to SOFC fabrication techniques, ceria coatings on metal substrates that protect against unwanted oxidation are investigated below.

5.3.1 *Experimental Details*

A nickel anti-dot film with initial and final PS diameters of 2 µm and 1 µm, respectively, was deposited onto one side of a YSZ single crystal, as before (c.f. Chapter 2). This

substrate was vertically dipped halfway into a Sm-doped ceria CELD electrolyte solution, and a potential was applied at -0.525 V vs. SCE for 1 hour. A thin film of ceria coated half of the cell, whereas the other half still had the nickel anti-dot film exposed. This sample was placed into a PLD system, where a 1 – 2 μm ceria film was deposited onto both its coated and uncoated areas. The PLD operated with a background oxygen partial pressure of 5 mtorr and at a substrate temperature of ~650 °C. SEM images are used to evaluate the oxidative state for the coated and uncoated regions.

5.3.2 *Results*

The CELD coated nickel anti-dot film before the PLD deposition is shown in Fig. 5.11a. Smooth and relatively crack-free, the deposition is nearly conformal, even over the occasional trapped PS sphere. The PLD deposition over the coated region appears similarly smooth, as in Fig. 5.11b, although there are more faceted features characteristic of crystalline ceria. Of particular note is the flatness of the area lying directly above the nickel anti-dot film. The cross section of the coated region is also shown in Fig. 5.11c. The border area between the CELD coated and uncoated regions after the PLD deposition is shown in Fig. 5.11c. There is a clear difference between the two, where the coated region is flat, like the original morphology, and the uncoated region has volume-expanded, noticeable by the smaller pore diameter. This volume expansion is from the nickel metal oxidizing to NiO during PLD operation.

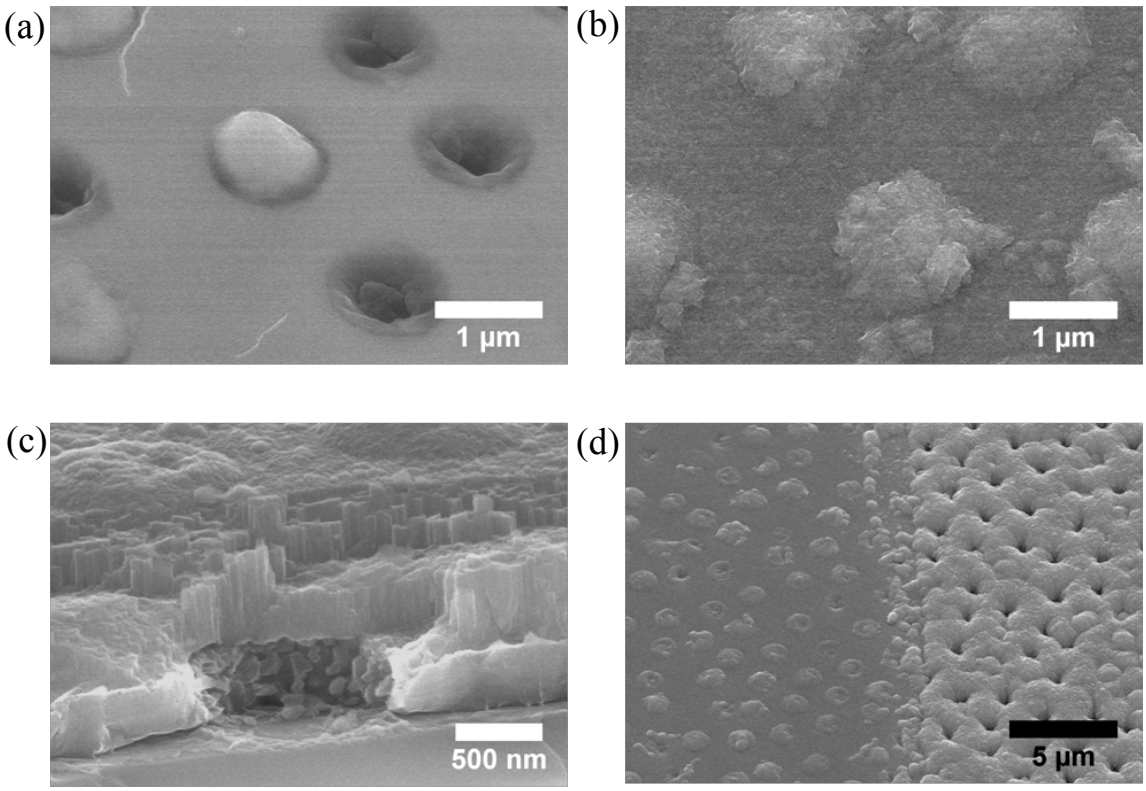

Fig. 5.11. SEM images of a thin film CELD ceria coating on a YSZ/Ni anti-dot substrate: (a) as-deposited; (b) the subsequent PLD top coating on the region that was previously coated by CELD ceria; (c) a cross-sectional view of the YSZ substrate/Ni anti-dot layer/CELD ceria layer/ PLD top coating layer; and (d) the PLD top coating showing the border between the previously coated region (left) and the uncoated region (right).

From these results, it can be concluded that the CELD ceria layer effectively prevents significant oxidation of the nickel metal. CELD could be used to treat metallic substrates before they are subjected to high temperature oxidizing conditions commonly used in SOFC fabrication techniques.

5.4 CELD Ceria Grown Directly on MIEC SOFC Cathode Substrates

In contrast to their anode counterparts, SOFC cathodes are commonly comprised of porous MIEC monoliths, typically with pervoskite-based crystal structures. Two such MIEC materials are $Ba_{0.5}Sr_{0.5}Co_{0.8}Fe_{0.2}O_{3-\delta}$ (BSCF) and $SrCo_{1-x}Nb_xO_{3-\delta}$ (SCN) [19, 122].

The mixed conduction is dominated by p-type electronic conduction in both material systems, and both exhibit non-trivial conductivity at room temperature and ambient pressure. This last characteristic, in particular, opens wide the possibility of utilizing BSCF and SCN as conducting substrates in a variety of configurations for CELD ceria. Most tantalizing is the possibility to make an entire cathode-electrolyte-anode SOFC assembly, beginning with the cathode. One can imagine depositing a thin film of ceria by CELD onto a self-supported, porous BSCF substrate, where densification of the ceria thin film could allow it to perform as the electrolyte in a SOFC. The top surface of this newly formed ceria electrolyte could then act as the substrate for subsequent anode fabrication, like the model electrodes from Chapters 2 and 3. This fuel cell fabrication scheme has the advantages of combining processing techniques that are naturally integrated with one another, as well as not requiring the characteristic high processing temperatures associated with more classical approaches.

Accordingly, the CELD of ceria onto BSCF substrates is investigated, with analogous (but not shown) results for SCN substrates.

5.4.1 *Substrate Preparation Details*

Dense and porous BSCF substrates were prepared for CELD studies. A standard powder process is employed for both, with a pore former used for the latter. BSCF powders are prepared by a nitrate-based sol-gel method, which utilizes EDTA and citric acid as complexing agents. The mixing bath is kept at temperatures around 80 °C, which induces gelation. The resulting sticky gel is heat treated at ~250 °C to remove residual organics. The blackened powders are then fully calcined at 950 °C to produce the desired pure

perovskite crystal phase. For dense substrates, this calcined powder is crushed by hand with a mortar and pestle, pressed into a pellet isostatically at 350 MPa, and then ultimately sintered at ~1050 °C. For porous substrates, the calcined powder is mixed in a 60:40 volumetric ratio with Cs_2SO_4, which acts as a pore former and is later removed by water immersion, and the two powders are crushed together in the mortar and pestle to ensure adequate mixing. This powder mixture is also isostatically pressed into a pellet, but sintered at ~800 °C, owing to the low melting temperature of the cesium sulfate salt (~1000 °C). The resulting pore sizes are on the order of a few microns.

The dense substrates are polished, using up to an 800 grit abrasive paper, and can be simply immersed into the CELD electrolyte solution as before. However, to encourage bridging of the pores by a thin ceria CELD layer and to discourage deposition inside the pores, the porous BSCF substrates are mounted to a glass slide by conducting copper tape, and infiltrated by viscous nail polish. The spontaneous capillary forces are sufficient for full infiltration of the pores. After the polish has hardened, the top surface is gradually planarized by 800 grit abrasive paper, and ultimately smoothed by 2 μm abrasive cloth (Scientific Instrument Services micro mesh cloth, 12000 grit). The result is a nanometer-scale smooth surface, with seamless interfaces between the nail polish-filled pores and the surrounding BSCF matrix, as in Fig. 5.12. Electrical contact with the external power supply is made via the underlying copper tape, a portion of which extends out from underneath the pellet. All conducting surfaces except the desired smoothed BSCF one are insulated from deposition by nail polish.

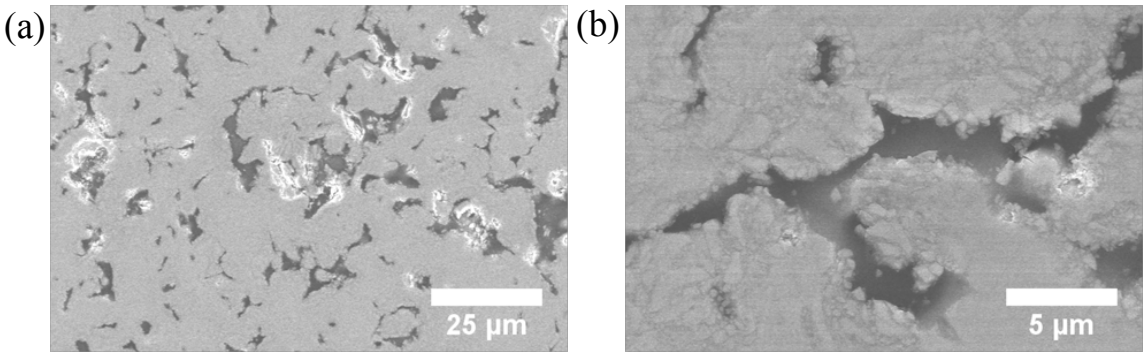

Fig. 5.12. SEM images of a porous BSCF substrate that has been infiltrated by viscous nail polish, which has since hardened. These images are taken after planarization by abrasive cloth. The isolated, dark regions are the hardened nail polish, surrounded by the lighter regions of sold BSCF.

5.4.2 *CELD Results and Discussion*

Figure 5.13 shows successful undoped ceria HSA deposition at 1.5 mA cm^{-2} for 5 minutes onto a dense BSCF substrate. The CELD undoped electrolyte solution used for this sample is slightly altered from the familiar composition—0.1M cerium nitrate with 0.1 M H_2O_2. The voltage response was abnormal in that it reached values of -2.2 V vs. SCE, which is much more negative than on regular metallic substrates. Highly uniform and slightly cracked, the familiar nano-needle/sheet growth can be seen. Fig. 5.13c and d reveal a cross-sectional piece of the deposit that was upended during subsequent handling of the sample. The 5 minute deposition produced a multiple-microns-thick coating on the BSCF, likely due to the high current density. The porous nature of the HSA deposit is clearly visualized in these images.

Deposition onto the porous BSCF substrate assembly is shown in Figure 5.14. Fig. 5.14a shows the sample immediately following deposition, with the nail polish still inside the BSCF pores. Fig. 5.14b-d show the sample after the nail polish has been

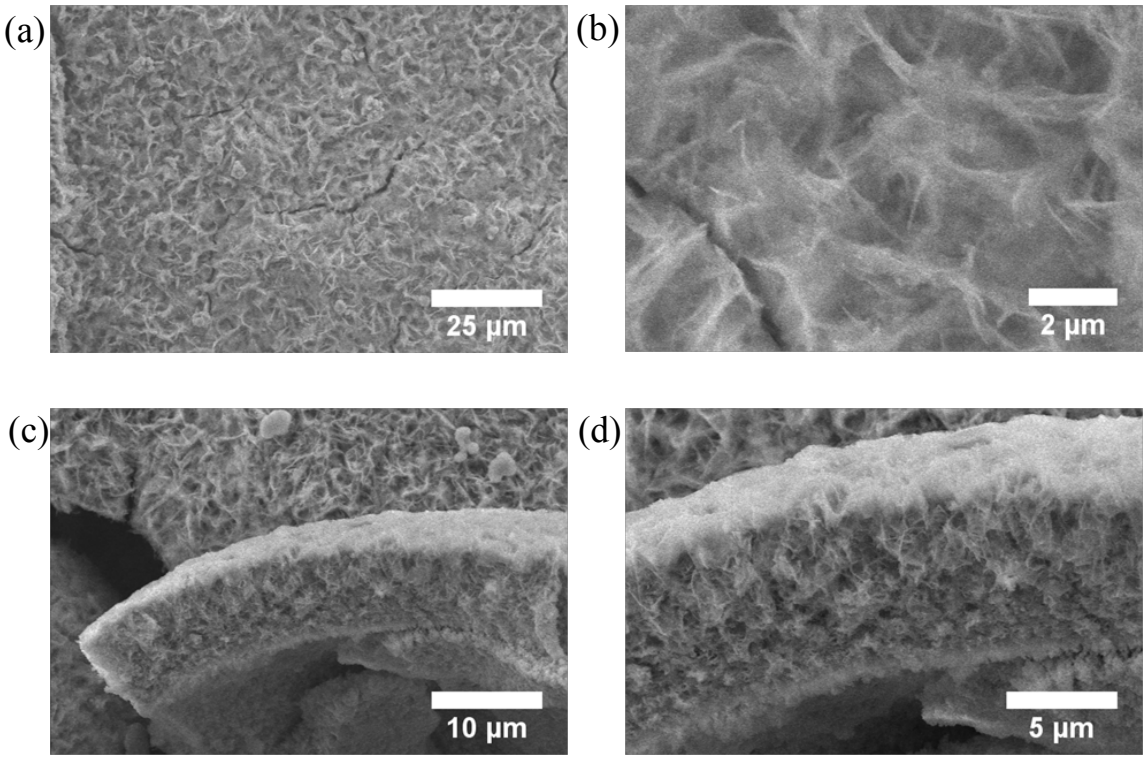

Fig. 5.13. As-deposited SEM images of undoped CELD ceria grown on a dense BSCF substrate at 1.5 mA cm^{-2} for 5 minutes, with a slightly more concentrated (0.1 M cerium nitrate) electrolyte with 0.1 M H_2O_2: (a) and (b) are top-down views; and (c) and (d) show an upended cross-section.

removed by acetone washing. Some of the smaller pores are successfully bridged by the thin ceria deposit, but as many of the BSCF pores are greater than 1 µm, they remain open and, therefore, gas permeable. This deposition is using the standard Sm-doped electrolyte solution with no hydrogen peroxide additive. Curiously, the applied voltage is only -0.5 V vs. SCE, which should produce a thin, planar film, a la the results obtained in Chapter 3. Furthermore, at a deposition time of only 1 minute without hydrogen peroxide, it is surprising that there is a discernable coating at all, much less one with the HSA microstructure.

To investigate this peculiarity, CV scans for nickel and BSCF substrates in the standard Sm-doped ceria electrolyte solution at 50 mV s^{-1} are compared in Figure 5.15.

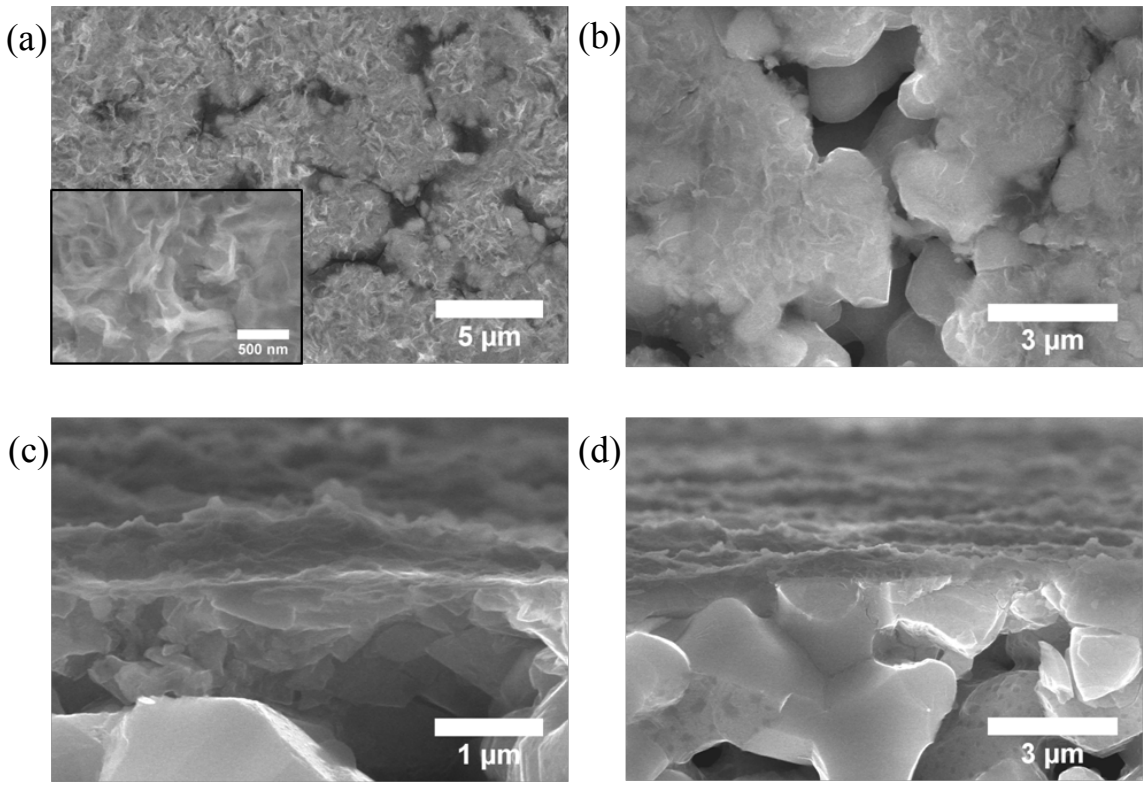

Fig. 5.14. SEM images of doped CELD ceria grown on a porous BSCF substrate at -0.5 V vs. SCE for 1 minute: (a) the as-deposited morphology with the nail polish still intact, and a closer view in the inset; (b) same as in (a), but with the nail polish removed; and (c) and (d) cross-sectional images showing some bridging of larger pores.

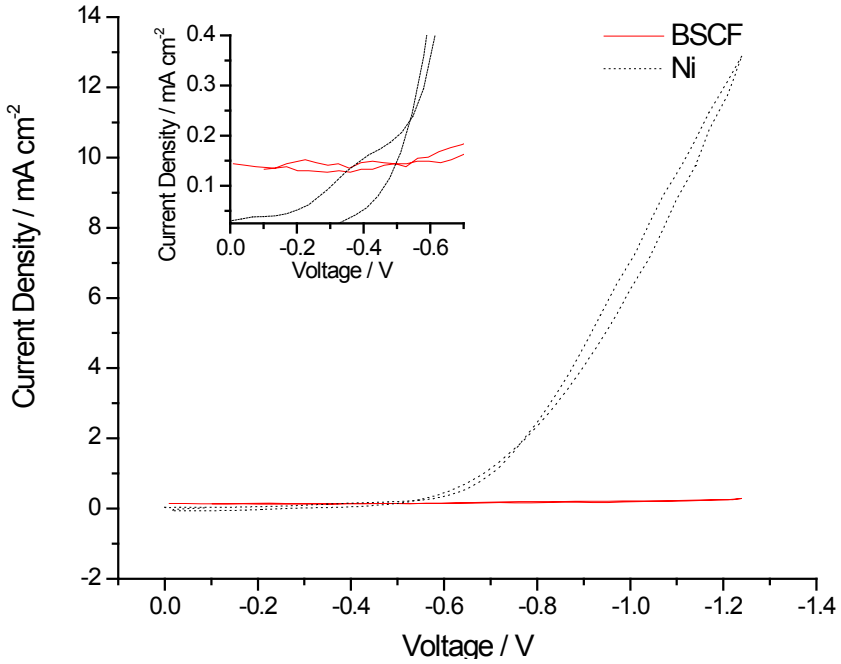

Fig. 5.15. CV scans for nickel and BSCF substrates in the standard doped electrolyte, with a scanning rate of 50 mV s^{-1}. Inset is a magnified view for the less negative potential range.

As previously discussed, the large current leg for the nickel substrate corresponds to the reduction of dissolved molecular oxygen and hydrogen gas evolution. As is clearly seen, BSCF does not exhibit such currents at the same voltages. However, BSCF does have a non-zero current at less negative voltages, significantly higher than the nickel substrate, shown in the inset of Fig. 5.15. With such a non-zero current, deposition should be able to occur at these lower voltages.

Indeed, Fig. 5.16a and c show top-down SEM images of films deposited in the Sm-doped ceria electrolyte solution for 30 seconds on porous BSCF at -0.2 V vs. SCE and no applied potential, respectively. When these porous BSCF substrates are removed from the CELD electrolyte solution, a distinctive deep blue/purple film appears, confirming deposition. Close inspection of the images in Figure 5.16 reveal slight cracks or tears in the thin films, even on top of nail polish-filled BSCF pores. After removing the nail polish by acetone washing and annealing at 700 °C for 10 hours under ambient air, some of the bridged areas are maintained, while others are punctured, as in Fig. 5.16b. There appears to be a simple correlation between the BSCF pore size and the ability of CELD coatings to bridge the pore. In an effect to boost the bridging capability of these thin films, eleven 30 second-long, subsequent depositions are performed at -0.65 V vs. SCE in the Sm-doped ceria electrolyte solution onto porous BSCF. The as-deposited results are shown in Fig. 5.16d, where some evidence of multiple depositions can be seen by layered tearing in certain areas. This effort does not sufficiently strengthen the deposited film, however, and the nail polish removal step introduced significant holes in the ceria film, as before.

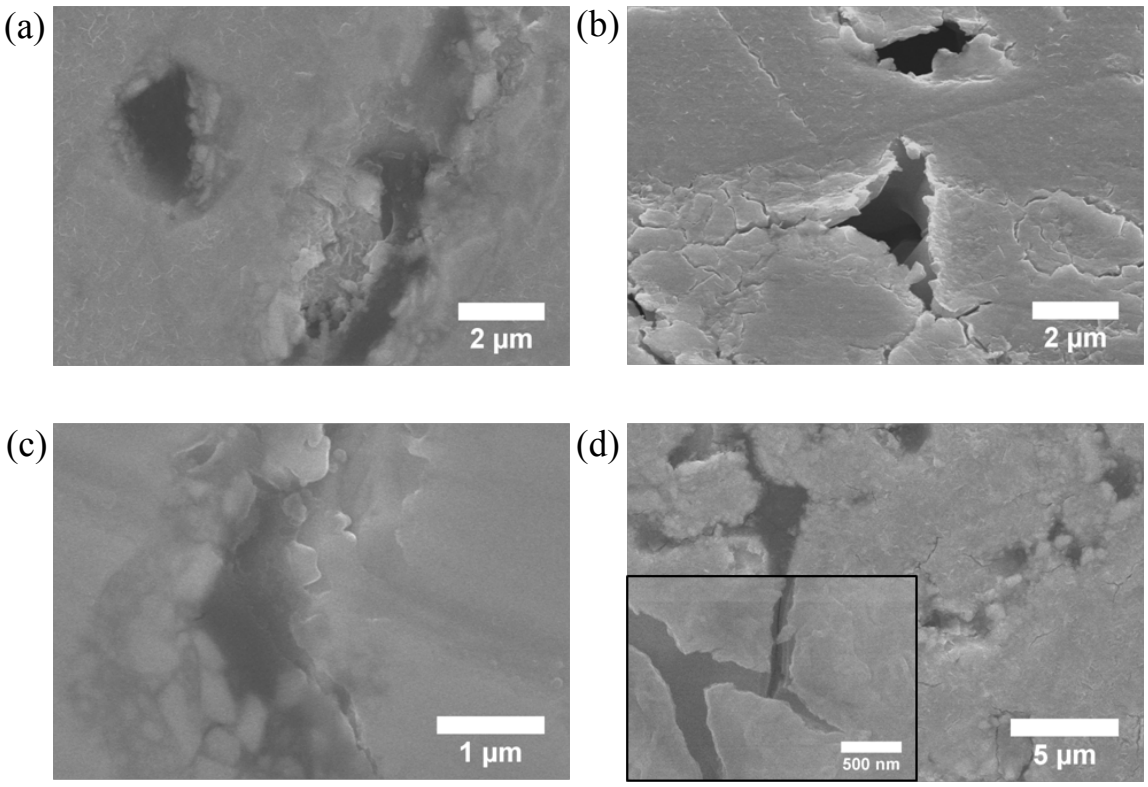

Fig. 5.16. SEM images of thin films of CELD ceria grown onto porous BSCF with the doped electrolyte: (a) and (b) at -0.2 V vs. SCE for 30 seconds, (a) as-deposited with the nail polish still intact (dark regions) and (b) after nail polish removal and annealing at 700 °C for 10 hours in air; (c) at no applied potential for 30 seconds, shown as-deposited; and (d) after eleven 30 second-long consecutive depositions at -0.65 V vs. SCE, shown as-deposited. The inset in (d) shows layered tearing, confirming multiple depositions.

A plausible explanation for this anomalous behavior is the oxygen electroreduction action of BSCF. The oxygen vacancy defect chemistry for an electron hole/oxygen ion MIEC can be depicted by the following equation:

$$O_O^X + 2h^{\cdot} \leftrightarrow \tfrac{1}{2}O_2(g) + V_O^{\cdot\cdot} \tag{5.3}$$

As the temperature increases, BSCF thermodynamically loses lattice oxygen to the atmosphere; as the temperature decreases, the opposite occurs—BSCF incorporates oxygen from its surroundings into its lattice. However, around room temperature, the kinetics of such incorporation are slow, meaning BSCF that has experienced any high temperatures will be essentially meta-stable at low temperatures seen later in time. This

incorporation reaction could be catalyzed when the BSCF is immersed into a CELD electrolyte solution, and connected to an electronic circuit. Noticing that the non-zero current in the BSCF CV of Fig. 5.15 is cathodic, the direction of current flow is consistent with what would be induced by Eqn. 5.3. However, this explanation offers no insight into why or how ceria is deposited. If it is assumed that the available oxygen vacancies on the surface of BSCF are isolated, i.e. it is unlikely that two vacancies are directly adjacent to each other in the crystal lattice, then only one oxygen atom would be incorporated at a time. For molecular oxygen, this would leave another atom available to aqueous hydrogen ions roaming in the acidic environment to produce a hydroxide ion. Then, the precipitation of cerium species could continue, as before.

There is also scant evidence of BSCF substrates catalyzing anomalous ceria structural growth. Microstructures reminiscent of the so-called nanosheaves of ref [123] and feathery, self-assembling fractal scaffoldings are found near the meniscus area of the sample from Figure 5.13. Some representative structures are pictured in Figure 5.17.

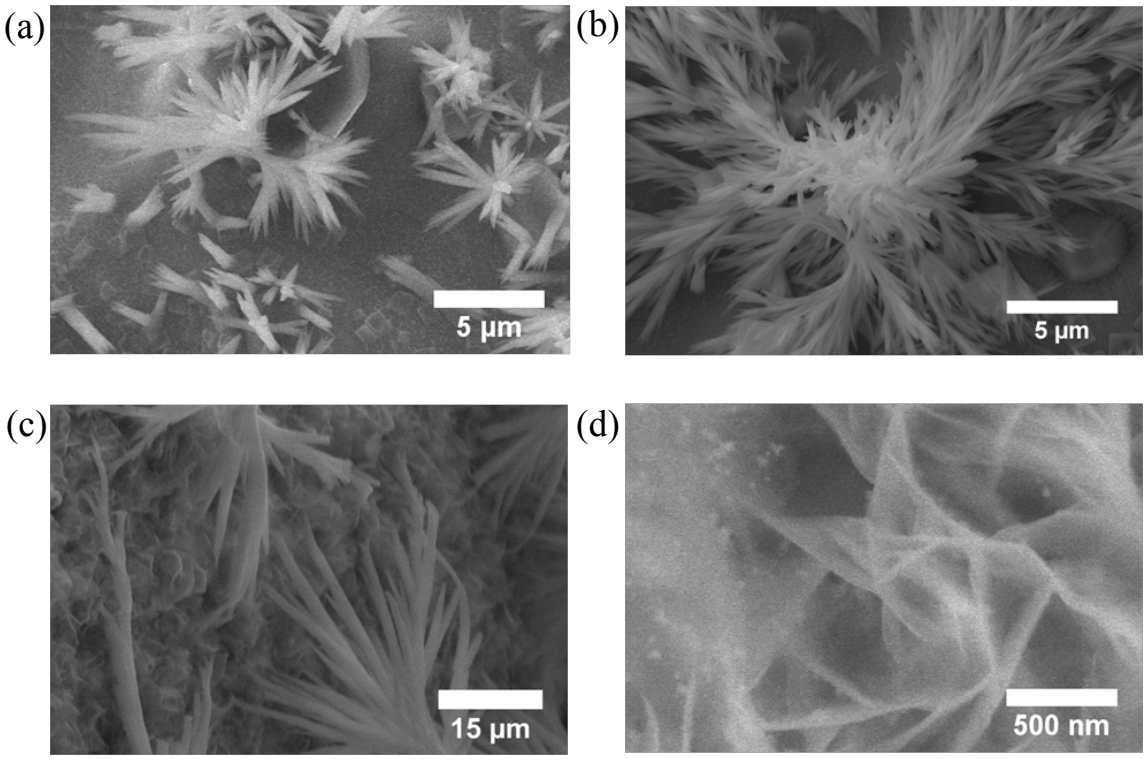

Fig. 5.17. SEM images of various structures deposited near the meniscus area for the sample from Fig. 5.13.